Journal of Power Sources 196 (2011) 4283–4289

Contents lists available at ScienceDirect

Journal of Power Sources

journal homepage: www.elsevier.com/locate/jpowsour

Influence of CrN-coating thickness on the corrosion resistance behaviour of aluminium-based bipolar plates

José Barranco[a,*], Félix Barreras[b], Antonio Lozano[b], Mario Maza[a]

[a] Univ. Zaragoza, Department of Mechanical Engineering, María de Luna 10, 50018 Zaragoza, Aragon, Spain
[b] LITEC, CSIC – Univ. Zaragoza, María de Luna 10, 50018 Zaragoza, Spain

ARTICLE INFO

Article history:
Received 30 July 2010
Received in revised form 29 October 2010
Accepted 15 November 2010
Available online 23 November 2010

Keywords:
PVD
Corrosion
Bipolar plates
PEMFC
Hydrogen

ABSTRACT

The electrical and corrosion properties of CrN-coated aluminium alloy Magnal-45 (Al-5083) probes have been evaluated, in order to assess their viability to be used as bipolar plates in polymer electrolyte fuel cells. To this end, ceramic micro-layers of chromium nitride (CrN) with different thicknesses (3, 4, and 5 μm) have been deposited on the surface of the Al alloy (Al-5083) using the physical vapour deposition (PVD) technique. A decrease in 2 orders of magnitude of I_{corr} values for the coated Al has been observed compared to the as-received Al-alloy when the probes have been exposed to simulated anodic conditions in a micro-reactor. On the other hand, when subjected to a cathodic-simulated environment, the Al–CrN probes with 3 μm and 4 μm coatings have shown a decrease in I_{corr} of one order of magnitude, while a variation of two orders of magnitude has also been obtained for the 5 μm coating.

1. Introduction

Light metals could be a suitable choice to be used as the base materials for bipolar plates (BP) in polymer electrolyte fuel cells, because they have an excellent thermal and electrical conductivity, high mechanical strength and their manufacturing is relatively easy. However, they are excessively susceptible to corrosion in the acid and humid environment of the operating fuel cells. In order to make them a viable option, they have to be protected with an appropriate coating that increases their resistance to corrosion while preserving the high conductivities. A wide variety of coating alternatives have been studied [1,2].

A large number of works have been devoted to enhance the low corrosion resistance of 304, 316L, 349 and 446 stainless steel (SS) [3–6]. Results indicate that SS shows an increase in the contact resistance value in a short period of time. At the same time, some material migration towards the membrane has been observed when tested in corrosive acid media. To overcome such limitations, different coating materials and methods have been considered. Nitrides, usually applied by physical vapour deposition (PVD), are possible candidates due to their good electrical properties [7–11]. However, additional surface treatments might be required. For example, chromium nitride coatings produce Cr-depleted regions where the corrosion resistance appears to be less compared to the base metal although with better electrical conductivity, together with zones of high Cr concentration where the corrosion protection is low due to galvanic pairs.

Due to the moderate manufacturing cost and low density, aluminium can be considered for BP applications in PEM fuel cells. However, this metal and its alloys get rapidly corroded in the typical fuel cell environment. In this case, metallic ions are released, migrating towards both catalyst layers and polymeric membrane, causing their contamination and, consequently, decreasing the fuel cell output [12]. Yet, coated-aluminium bipolar plates may overcome such limitations, reaching DOE targets. In this sense, coatings have to provide good electrical conductivity, as well as a similar value of the thermal expansion coefficient to that of the metal substrate. At the same time, coatings must exhibit a suitable adherence to the base metal in order to prevent its exposure to the corrosive media. Another important parameter to be checked in bipolar plates is the interfacial contact resistance (ICR), which may be either increased or decreased by the coatings, thus altering the PEM fuel cell performance. Degradation of the resistance values can be mainly due to coating process failures, roughness of the external coating surface, or to the intrinsic characteristics of the coating material.

Lee et al. [13] applied a coating of YZU001, a diamond-like material, on 5052 aluminium and 316L stainless steel BPs using PVD, in order to compare their performance with graphite plates. They manufactured three different single cells to measure contact resistance as well as cell performance. Results indicated that the coated Al-5052 and SS-316L showed better performance than the

* Corresponding author. Tel.: +34 976 506 520; fax: +34 976 506 644.
E-mail address: barranco@litec.csic.es (J. Barranco).

0378-7753/$ – see front matter © 2010 Elsevier B.V. All rights reserved.
doi:10.1016/j.jpowsour.2010.11.069

graphite cell at low voltage, although the later exhibited longer average life. They also reported that the natural passive film on the SS-316L plate resulted in a better corrosion resistance than that of the coated Al-5052 plate. However, the former presented higher ICR values thus reducing the cell performance. The Al-coated plates showed better single cell performance and contact resistance, although the cell lifetime was shorter. Hu et al. [14] reported the improvement on corrosion resistance of an aluminium-based composite BP coated with chromium nitride (CrN) by magnetron sputtering. Potentiodynamic polarization curves confirmed that the CrN-coated composite shows not only much lower susceptibility to pitting corrosion but also a significant increase in the corrosion resistance with respect to untreated composites when immersed in a corrosive solution.

In the present research, the influence of the thickness of a CrN single layer ceramic coating deposited on aluminium probes using cathodic arc evaporation physical vapour deposition (CAE-PVD) on the electrical and corrosion resistance properties has been evaluated. The coated probes have been exposed to conditions that closely simulate the typical environment of both anode and cathode sides in real PEM fuel cells, and their corrosion resistance has been analysed by electrochemical polarization tests. ICR measurements have been performed, and the surface morphology of the coatings before and after the corrosion tests has been analysed using scanning electron microscopy (SEM). The chemical composition of the coatings has also been verified using glow discharge optical emission spectroscopy (GD-OES).

2. Experimental procedure

2.1. Coating process

Prior to performing the coating of the Al-5083 alloys, all the samples have been mirror-polished first with a SiC paper and subsequently using diamond paste in order to obtained a final roughness of Ra < 0.7 μm. Afterwards, the substrates have been introduced in an alkaline bath, thoroughly rinsed in deionised water and ultrasonically washed in acetone in order to clean up the surface from any organic substances. Before coating, ion cleaning has been carried out to avoid any contaminant, and to improve the coating adhesion by removing the Al natural oxide layer. Inert argon has been used in the ion cleaning process. All the coatings have been deposited on a Cr base layer to enhance the adhesion strength between coating and substrate. The Al alloys have been coated with CrN single layers of different thicknesses (3 μm, 4 μm, and 5 μm) using a METAPLAS IONON MZR 322 machine equipped with 6 arc evaporators and a 500 mm × 500 mm × 500 mm vacuum chamber. Voltage bias, temperature and vacuum pressure have been fixed for all the coating processes at −50 V, 400 °C, and 0.006 mbar, respectively.

2.2. Surface characterization

Different experimental techniques have been applied to characterize the coated Al-probes. In order to evaluate corrosion resistance, surface roughness and composition, the probes have been analysed before and after polarization tests by scanning electron microscopy (SEM) with energy dispersive X-rays (EDX), using a Hitachi S-3400 N with a Röntec XFlash Si(Li) EDX analyzer. Chemical in-depth composition profiles of the coatings have also been performed by GD-OES, using a JY 10000 RF instrument.

2.3. Electrochemical measurements

The corrosion behaviour of the samples has been measured in acid media corresponding to a 0.5 M H_2SO_4 + 2 ppm HF solution at 70 °C by means of potentiostatic and linear sweep voltammetry (LSV). A stream of either hydrogen or oxygen was continuously bubbled to the solutions in order to simulate actual PEM fuel cell anode and cathode environments. An electrochemical reactor with a conventional three electrode system has been used in which the reference electrode was Ag/AgCl (0.210 V vs. RHE). A carbon sheet (1 mm thick) and the coated samples have been used as the counter and working electrodes, respectively. For all Al-coated probes a corrosion surface area of 1 cm^2 has been considered. Due to the fact that each probe has been coated only on one side, the uncoated face has been protected from the acid solution with an epoxy resin. In this study, all potentials are referred to the Ag/AgCl electrode. Measurements have been obtained using an Autolab Instrument potentiostat/galvanostat (PGSTA 302). LSV has been used to compare the general electrochemical behaviour of the samples. In this test, the samples were stabilized at an open circuit potential (OCP) for 2 min. In the same way as in previous works [12,15], the potential has been then swept from −0.3 V vs. OCP to +0.3 V vs. OCP at a scanning rate of 1.5 mV s^{-1}.

To study the samples behaviour under typical PEM fuel cell cathode potentials, short-term potentiostatic experiments have been performed. In these measurements samples were stabilized at OCP for 10 min, then a specific potential of 0.5 V vs. Ag/AgCl was applied.

2.4. Interfacial contact resistance

The interfacial contact resistance (ICR) measurements for all the Al-coated alloys have been carried out at room temperature using an Itech DC electronic load and a True RMS multimeter by a method similar to that proposed by Davies et al. [16]. An electrical current of 1 A was supplied between two copper thin plates placing one piece of gas diffusion layer (ELAT® V2.1) and the Al-coated probes between them. The total voltage drop between the copper plates was monitored while the compaction force was gradually increased from 15 N cm^{-2} to 170 N cm^{-2} using an Intron 5565 hydraulic press. This total voltage drop is the result of the sum of all the interfacial contact resistances, and the intrinsic resistance of each one of the materials used

$$(R_T = R_{Cu/GDL} + R_{Coating/GDL} + R_{Al/Cu} + R_M)$$

where R_M is the sum of all the intrinsic resistances. Thus, the ICR value of the carbon cloth and the CrN coatings ($R_{Coating/GDL}$) can be obtained by subtracting the separately measured values of the rest of the resistances, for each compaction force.

3. Results and discussion

3.1. Surface analysis

Fig. 1a–c shows the chemical in-depth composition profiles for different CrN–coated Al alloys. As can be observed, for the first 0.1 μm, concentrations of oxygen and carbon drastically decrease from 10% down to 0% atomic. This latter value is maintained for the rest of the depth profiling. This behaviour is common when the analysed surfaces are contaminated by the atmospheric environment. However, a more remarkable fact is that for the different probes all the concentrations of Cr, N, and Al remain constant with a fixed ratio of 70:30:0% atomic, during the coating process and along the whole depth profile. Thus, it can be inferred that the chemical reaction between Cr and N is the main process that occurs during the coating synthesis.

As can be observed in Fig. 2, the formation of pinholes and macro-defects, such as droplets and craters in the PVD coating is nearly impossible to avoid despite all the efforts in polishing the surface of the Al alloys before the coating process. In a pre-

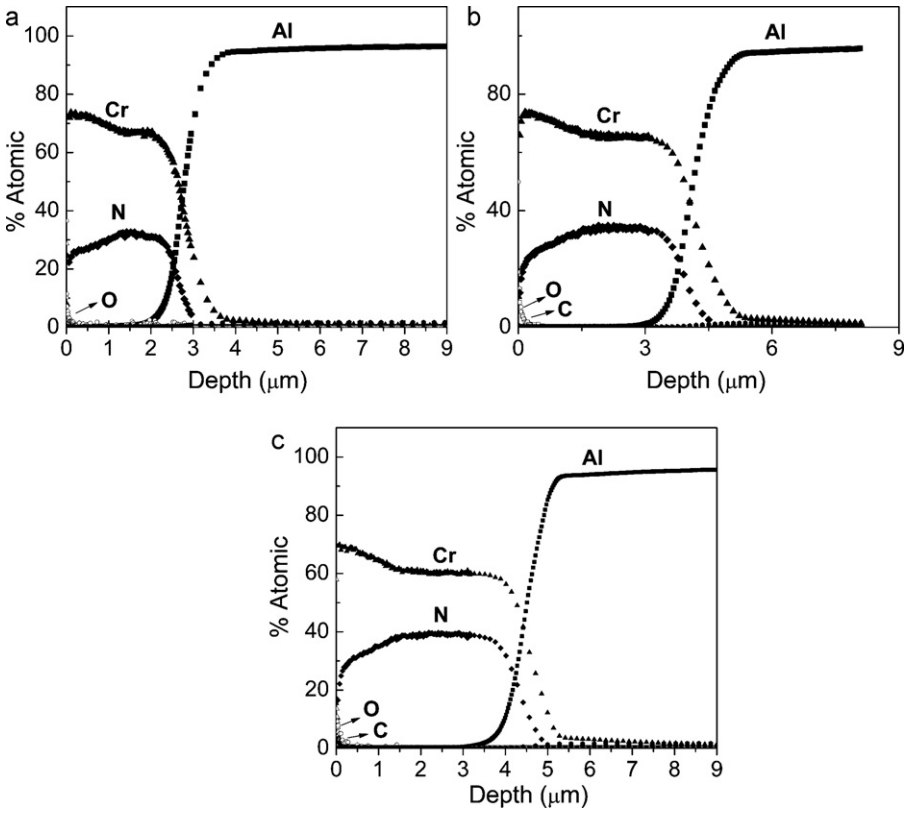

Fig. 1. Composition-depth obtained with glow-discharge optical emission spectroscopy (GD-OES): (a) CrN-3 μm, (b) CrN-4 μm and (c) CrN-5 μm coatings.

vious work related to CrN and CrN/ZrN coatings [17], it has been demonstrated that even for a substrate surface roughness lower than the one achieved in this work (Ra < 0.2 μm), the existence of such defects was clear in all the samples analysed. This result is consistent with that found by Korhonen [18], who argued that although various techniques can be used to minimize the number of pinholes, they cannot be totally eliminated. SEM cross-sectional views of the CrN coatings deposited on the Al alloy substrates are depicted in Fig. 3a–c. As can be observed, the general growth morphology of the coatings is in tubular column type. All the coatings have shown a preferential orientation to form a dense tubular column of CrN grains deposited perpendicularly to the substrate surface. As can also be seen, the actual coating thicknesses measured in cross-sectional SEM micrographs are very similar to those expected according to the in-depth composition profiles obtained with the GD-OES technique already discussed. Table 1 depicts the roughness value measured for each coated sample. As can be observed, the thicker the CrN coating, the denser the tubular column grain growth, reducing the porosity of the coated surfaces.

3.2. Interfacial contact resistance

The ICR measurements for the different coated samples and Al alloy are plotted in Fig. 4. ICR data for a commercial stainless steel SS-304 has been added for comparison, and also to check the validity of the experimental setup. It is found that ICR values decrease with increasing compaction force for all the samples mainly due to an increase in the contact area between the surface sample and the carbon cloth. The ICR values of the stainless steel and the Al-alloy for a compaction force of 135 N cm^{-2} are 116 and 34 mΩ cm^2, respectively. The ICR values of the coated Al samples are lower than those obtained for the uncoated Al-base metal. The inset in Fig. 4 shows detailed ICR values of the coated samples. CrN-3 μm and CrN-4 μm samples show similar ICR values, 8 and 8.5 mΩ cm^2 at 135 N cm^{-2}, respectively. The CrN-5 μm shows the lower contact resistance for the different compaction forces measured, e.g. 6 mΩ cm^2 at 135 N cm^{-2}. This behaviour may be ascribed to differences in the surface roughness of the samples (see Table 1). The slope of the ICR curves decreases as the sample roughness increases. Thus, the effect of the compaction force becomes more evident for increasing roughness.

It should be noted that due to the presence of several pitting holes produced by corrosion, measurements of ICR after polarization studies reported very inconsistent results. As the size and distribution of the holes is very uneven from one sample to another, the uncertainty in the contact area is very large and measurements become unreliable.

3.3. Polarization curves

The potentiodynamic curves of the coated compared to the uncoated Al alloy at anodic and cathodic environments are shown in Fig. 5a and b, respectively. It can be noticed that regardless of the environment, the corrosion potential (E_{corr}) of the coated samples slightly shifts towards more positive values. However, more noticeable is the decrease in corrosion current densities (I_{corr}) obtained for the coated samples. Such decreases are of three orders of magnitude when working in anode conditions. Meanwhile, at cathodic conditions, a decrease of one order of magnitude for the CrN-3 μm and CrN-4 μm samples, and of three orders of magnitude for the CrN-5 μm sample are obtained. Table 2 depicts the kinetics parameters involved in the corrosion processes, obtained from the polarization curves. Among them, the polarization resistance (R_p), measured from the extrapolation of the anodic and cathodic branches in the tafel regions, is the parameter that best correlates with corrosion resistance. Thus, high R_p of the sample implies high corrosion resistance while low R_p means low corrosion resistance. The results show that coating the Al alloys using the PVD technique,

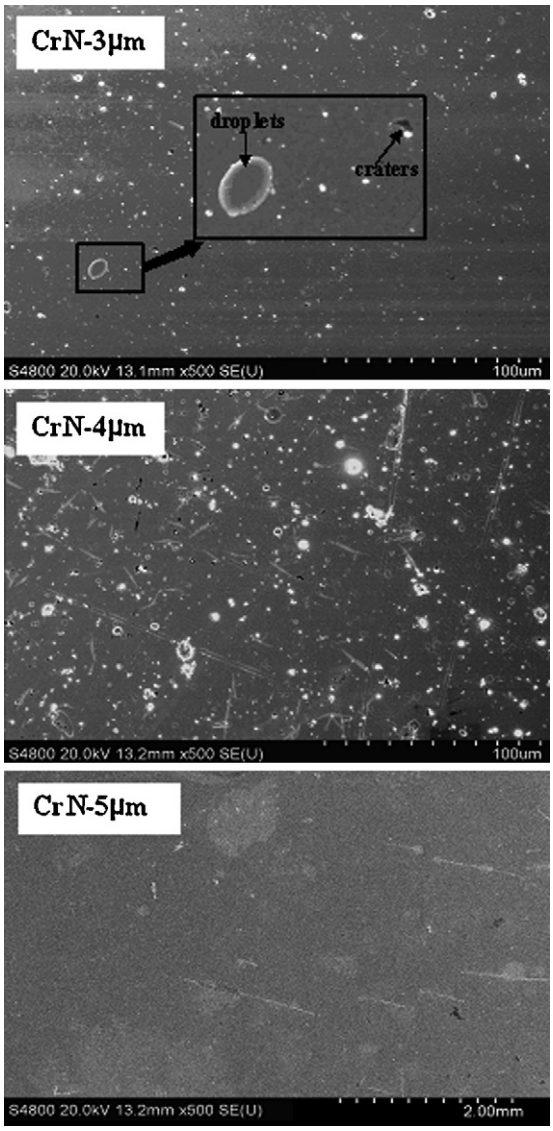

Fig. 2. Planar view of SEM micrographs for different CrN coatings.

greatly improves the corrosion resistance properties. Compared to the uncoated alloy, the R_p values are increased by two orders of magnitude in the anodic environment, and between two and three orders of magnitudes in a more aggressive cathodic environment.

Potentiostatic polarization tests obtained in a solution bubbled with oxygen are depicted in Fig. 6, showing a different behaviour for each type of coating. The potentiostatic curve for the CrN-3 μm Al-coated sample shows an initial increase in current density due to the oxidation of the CrN coating layer. Moreover, as the corrosion of the CrN surface increases, the presence of defects may increase and, once the solution reaches the substrate, aluminium oxide starts to grow, as shown by the initial drop in the current density–time transient (i/t). The subsequent steady-state at a current density value

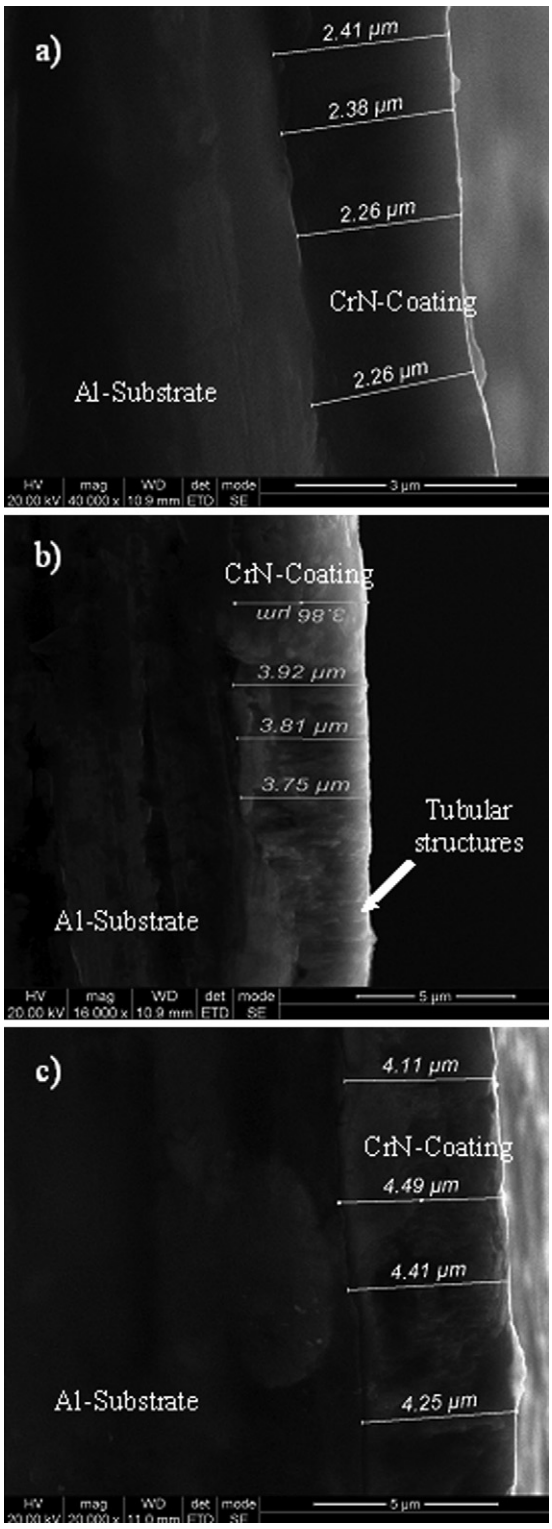

Fig. 3. Cross sectional SEM micrographs for coatings of different thickness, showing the tubular CrN growing morphology: (a) 3 μm, (b) 4 μm and (c) 5 μm.

Table 1
Roughness values measured for each coated sample.

Samples	Ra (nm)[a]	Rq (nm)[b]
CrN-3 μm	70 ± 10	110 ± 20
CrN-4 μm	60 ± 10	90 ± 60
CrN-5 μm	50 ± 10	70 ± 15

[a] Arithmetic average values.
[b] Root mean squared values.

of 0.39 mA cm^{-2} may be a consequence of the ratio between the kinetics of formation of aluminium oxide and its dissolution. The i/t transient behaviour for the uncoated Al alloy is quite similar to that of the CrN-3 μm Al-coated sample reaching current densities of 0.40 mA cm^{-2}. However, the initial drop for the coated sample is delayed, due to the initial slow corrosion rate of the CrN layer. It has also been verified that the uncoated Al alloy shows a gen-

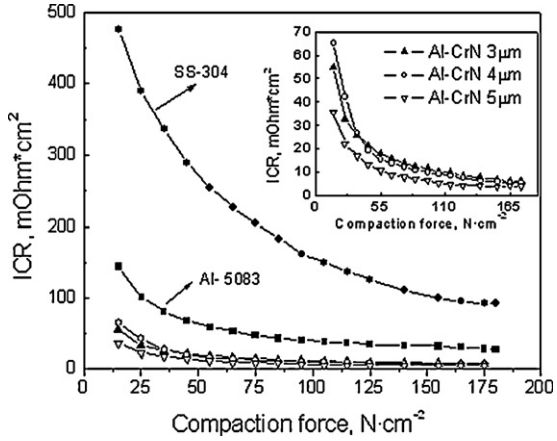

Fig. 4. Interfacial contact resistance (ICR) between coated or uncoated samples and carbon paper as a function of compaction force.

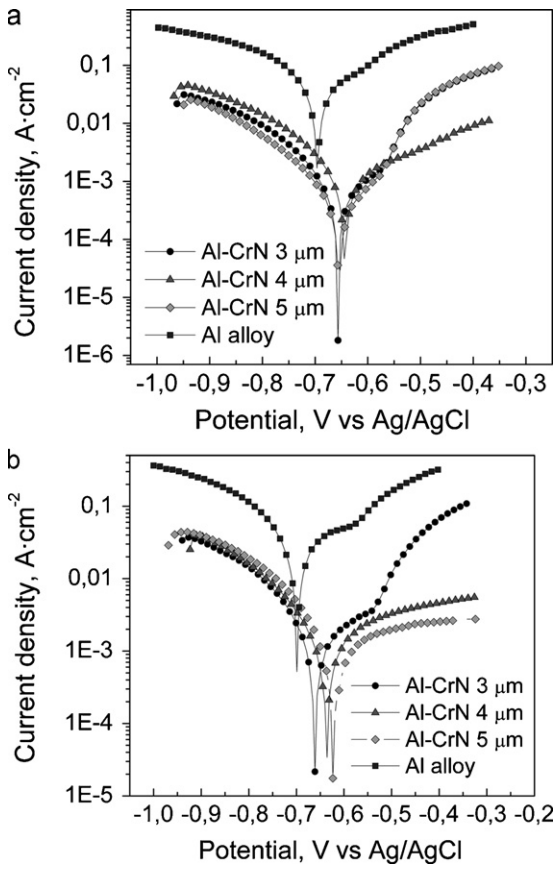

Fig. 5. Potentiodynamic polarization curves for uncoated Al alloy and Al–CrN coated samples: (a) anodic environment (0.5 M H_2SO_4 + 2 ppm HF, 70 °C, H_2 bubbled) and (b) cathodic environment (0.5 M H_2SO_4 + 2 ppm HF, 70 °C, O_2 bubbled).

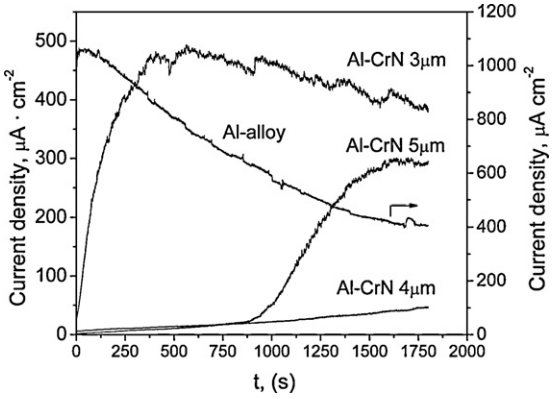

Fig. 6. Potentiostatic polarization curves for the uncoated and CrN-coated samples for cathodic environments (O_2 bubbling). Other conditions are: acid solution of H_2SO_4 0.5 M + 2 ppm HF, 70 °C, 0.5 V vs. Ag/AgCl (0.7 V vs. NHE).

eral corrosion process. The metal is corroded by dissolution of the bulk, not showing localized corrosion defects such as pits, cracks or pinholes. A similar corrosion behaviour has been obtained for both the CrN-3 μm coated Al sample and the uncoated Al alloy. This is somehow unexpected, due to the insensitivity of transition metal nitride coatings to chemical attack [19,20]. However, the similar corrosion behaviour could be explained by the presence of surface defects, such as pinholes or micro-cracks created during the coating corrosion processes, which may serve as solution-paths favouring the substrate corrosion.

The initial trend of the i/t transient is the same for the CrN-4 μm and CrN-5 μm coated samples. The coating effect on the current density shows very low corrosion kinetics, due to the slow decrease in surface roughness of the coating layer with increasing thickness. At steady-state the current density value was 0.47 mA cm^{-2}. However, the CrN-5 μm sample shows a similar pattern to that obtained for the CrN-4 μm coating during 900 s. After this, a steep increase of the current density has been observed. As will be discussed later, this behaviour may be a consequence of the compressive stress in the coating, which might yield stress–corrosion in this aggressive environment [21].

Fig. 7a–c shows SEM micrographs of the planar views for the CrN-3 μm, CrN-4 μm and CrN-5 μm Al-coated samples after the potentiostatic polarization tests in 0.5 M H_2SO_4 + 2 ppm HF (oxygen bubbled) solution at 70 °C. As can be observed in Fig. 7a, after 1800 s of potentiostatic test, the surface of the CrN-3 μm coating shows degradation evidences in the form of pitting corrosion. This type of local failures is normally developed when the protective layer does not corrode homogeneously, but only in preferential zones such as coating defects, growing solution-paths through pores, or pinholes. Once the solution reaches the substrate, the potentiostatic curve depicts a similar behaviour than that shown by the uncoated substrate, as discussed previously. In the micrographs, it can be seen how the pits are homogeneously distributed all over the surface with a pit size around 400 μm. Moreover, the cross-sectional SEM insert in Fig. 7a shows how the symmetry of the CrN colum-

Table 2
Corrosion potentials (E_{corr}), corrosion current densities (I_{corr}), and polarization resistances (R_p) measured for uncoated and coated aluminium probes during corrosion tests. Experimental conditions are: acid media solution 0.5 M H_2SO_4 + 2 ppm HF, bubbling H_2 (anodic environment) or O_2 (cathodic environment), scanning rate 0.0015 V s^{-1}, temperature 70 °C.

	I_{corr} (A cm^{-2})	E_{corr} (V)	R_p (Ω)	I_{corr} (A cm^{-2})	E_{corr} (V)	R_p (Ω)
Anodic conditions (H_2 bubbling)				Cathodic conditions (O_2 bubbling)		
Al Magnal-45	1.915×10^{-3}	−0.697	1.953×10^{-2}	1.038×10^{-3}	−0.699	9.984×10^{-3}
Al–CrN 3 μm	5.475×10^{-5}	−0.656	1.045	1.292×10^{-4}	−0.662	6.378×10^{-1}
Al–CrN 4 μm	1.885×10^{-5}	−0.642	1.402	1.956×10^{-4}	−0.636	1.89
Al–CrN 5 μm	5.742×10^{-5}	−0.655	2.107	7.912×10^{-5}	−0.623	1.144

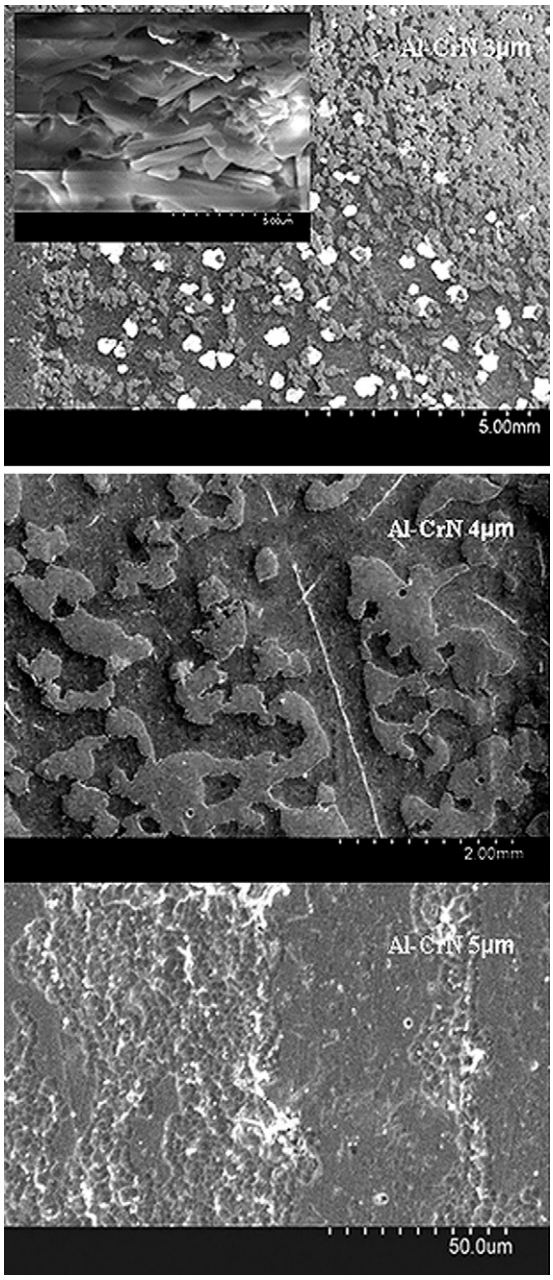

Fig. 7. Planar views of SEM micrographs for the CrN-3 μm, CrN-4 μm and CrN-5 μm Al-coated samples after potentiostatic polarization tests in 0.5 M H_2SO_4 + 2 ppm HF (oxygen bubbled) solution at 70 °C.

nar growth disappears as the Al substrate dissolves. Due to the fact that the CrN coating shows higher corrosion resistance, it can be concluded that it may act as the cathode and the Al substrate as the anode in a galvanic corrosion that easily starts when the solution reaches the substrate surface. Thus, the CrN tubular structures detach from the substrate from where they grew. This may be the reason why tubular CrN structures showed a non-homogeneous orientation after the polarization experiments. CrN-4 μm coatings have shown different corrosion morphology. In this case the coating provided the substrate a good protection against corrosion, mainly due to the denser tubular growth of the CrN specimen, decreasing the porosity of the layer. As can be observed in Fig. 7b, the corrosion morphology shows no evident pits or craters on the Al-base substrate. However, the CrN layer shows clear damages on the surface, due to the corrosion processes. A decrease of 2 μm in the thickness of the chromium nitride layer has been observed in the surface defects zones. However, Cr-5 μm coatings showed very different corrosion behaviour despite its reduced surface porosity. As depicted in Fig. 7c, the layer shows micro-crack diffusion over the surface, which provided solution-paths that reached the substrate. Moreover, once the micro-cracks are formed, internal defects which were covered by the dense CrN layer appear in the form of micro-pits, which accelerate the substrate corrosion. At this stage, the potentiostatic curve should behave as that for the uncoated Al, as discussed in Fig. 6. This behaviour may be consistent with the idea that the parameters used during the PVD process caused compressive stress in the CrN-5 μm coating which resulted in stress–corrosion cracking and the subsequent failure of the coating when exposed to a corrosive environment. Although not shown here, EDX analysis confirmed oxide formation, such as AlO_3. This is consistent with the results already obtained in previous works with the same Al alloys [17].

4. Conclusions

Al-5083 alloys have been protected with CrN coatings of different thickness and their corrosion resistance behaviour has been studied by LSV and potentiostatic techniques. Polarization curves have shown an increase in the corrosion resistance of all the CrN–Al samples at both anode and cathode conditions. Compared to the uncoated probes, the R_p values of the coated samples are increased by two orders of magnitude in the anodic environment, and between two and three orders of magnitudes in a more aggressive cathodic environment. At the same time, the interfacial corrosion resistance of the coated sample decreases significantly with decreasing coating roughness. Even when I_{corr} values are decreased by one or two orders of magnitude when CrN coatings are used, they are still significantly high to be sure that the coating is protecting the aluminium matrix efficiently. Besides, several corrosion pitting holes with uneven sizes have been observed in the samples after the polarization studies. Their presence prevented reliable post ICR analysis. For all these reasons, the PVD CrN coatings on Al used in this work might not be a suitable option for use in bipolar plates unless formation of pitting holes is eliminated.

Acknowledgements

The authors wish to thank the Centre of Advanced Surface Engineering (AIN) for the coating of the Al alloys. This research has been partially funded by the Spanish Ministry of Science and Innovation under projects CIT-370000-2008-11, ENE2008-06697-C04-01/CON, and ENE2009-14750-C05-02/CON. Authors are indebted to the referee. The points and concerns addressed during the reviewing process have helped to improve the final quality of the paper.

References

[1] A. Hermann, T. Chaudhuri, P. Spagnol, Int. J. Hydrogen Energy 30 (2005) 1297–1302.
[2] A.A. Renato, L.O. Mara Cristina, Gerhard Ett, Volkmar Ett, Int. J. Hydrogen Energy 35 (2010) 1–16.
[3] R.C. Makkus, A.H.H. Janssen, F.A. de Bruijn, R.K.A.M. Mallant, J. Power Sources 86 (2000) 5–9.
[4] D.P. Davies, P.L. Adcok, M. Turpin, S.J. Rowen, J. Power Sources 86 (2000) 237.
[5] H. Wang, J.A. Turner, J. Power Sources 128 (2004) 193.
[6] R.F. Silva, A. Pozio, J. Fuel Cell Sci. Technol. 4 (2007) 116.
[7] R. Tian, J. Sun, L. Wang, Int. J. Hydrogen Energy 21 (2006) 1874–1878.
[8] H.Y. Lee, S.H. Lee, J.H. Kim, M.C. Kim, D.M. Wee, Int. J. Hydrogen Energy 33 (2008) 4171–4177.
[9] H. Wang, M.P. Brady, G. Teeter, J.A. Turner, J. Power Sources 138 (2004) 86–93.
[10] Y. Wang, D.O. Northwood, Int. J. Hydrogen Energy 32 (2007) 895–902.
[11] H. Wang, M.P. Brady, K.L. More, H.M. Meyer III, J.A. Turner, J. Power Sources 138 (2004) 79–85.

[12] S.J. Lee, C.H. Huang, Y.P. Chen, J. Mater. Process. Technol. 140 (2003) 688–693.
[13] S.-J. Lee, C.-H. Huang, J.-J. Lai, Y.-P. Chen, J. Power Sources 131 (2004) 162–168.
[14] J. Hu, T.B. Li, H.L. Wang, W.C. Ren, Mater. Lett. 62 (2008) 1715–1717.
[15] S. Joseph, J.C. McClure, P.J. Sebastian, J. Moreira, E. Valenzuela, J. Power Sources 177 (2008) 161–166.
[16] D.P. Davies, P.L. Adcok, M. Turpin, S.J. Rowen, J. Appl. Electrochem. 30 (2000) 101–105.
[17] J. Barranco, F. Barreras, A. Lozano, A.M. Lopez, V. Roda, J. Martín, M. Maza, G.G. Fuentes, E. Almandoz, Int. J. Hydrogen Energy 35 (2010) 11489–11498.
[18] A.S. Korhonen, Vacuum 45 (1994) 1030–1034.
[19] I. Milosev, B. Navinsek, H.H. Strehblow, Julich (1995).
[20] H.W. Wang, M.M. Stack, S.B. Lyon, P. Hovsepian, W.-D. Münz, Surf. Coat. Technol. 126 (2000) 279–287.
[21] P.E. Hovsepian, D.B. Lewis, W.D. Münz, S.B. Lyon, M. Tomlinson, Surf. Coat. Technol. 535 (1999) 120–121.